Ultrafast photochemistry of free-base porphyrin: A theoretical investigation of B → Q internal conversion mediated by dark states †

Konstantin Falahati, Carsten Hamerla, Miquel Huix-Rotllant, Irene Burghardt

▶ **To cite this version:**

HAL Id: hal-02079633

https://amu.hal.science/hal-02079633

Submitted on 26 Mar 2019

Ultrafast photochemistry of free-base porphyrin: A theoretical investigation of $B \rightarrow Q$ internal conversion mediated by dark states[†]

Konstantin Falahati,[a] Carsten Hamerla,[a] Miquel Huix-Rotllant,[*b] and Irene Burghardt[*a]

We examine the mechanism of ultrafast internal conversion between the B band (Soret band) and the Q band in porphine (H_2P), the prototypical free-base porphyrin, using electronic structure studies and on-the-fly surface-hopping nonadiabatic dynamics. Our study highlights the crucial role of dark states within the N band which are found to mediate B/Q state transfer, necessitating a treatment beyond Gouterman's classic four-orbital model. The sequential $B \rightarrow N \rightarrow Q$ pathway dominates largely over the direct $B \rightarrow Q$ pathway which is found to be energetically unfavorable. Potential energy surface cuts and conical intersections between excited states are determined by TDDFT and validated by CASSCF/CASPT2 calculations. Both the static analysis and on-the-fly surface-hopping calculations suggest a pathway which involves minor structural deformations via in-plane vibrations. The $B \rightarrow N$ conversion is a barrierless adiabatic process occurring within ~20 fs, while the subsequent $N \rightarrow Q$ conversion occurs via a conical intersection within ~100 fs, in agreement with time-resolved experiments for porphine and related free base porphyrins. Furthermore, evidence for both sequential and direct transfer to the Q_x and Q_y states is obtained.

1 Introduction

Porphyrin-based compounds are of key importance in biology, bioengineering, and the design of chemosensors and functional nanostructures.[1–5] Notably, porphyrins represent one of the most important classes of water-soluble pigments found in hemeproteins, chlorophylls and cytochromes, where they exert various functions ranging from oxygen storage to electron and energy transfer.[3,6,7] The unique features of porphyrin photochemistry are determined both by their optical properties and their distinct molecular geometry. These features can be tuned in a variety of ways by substitution at the skeletal periphery or by incorporating metals.[8–13] The electronic properties of these heterocyclic tetrapyrrolic pigments also play a key role in the formation of aggregates[14] and their functionalization in the context of light-harvesting, e.g. in solar cells, or as potential agents in photodynamic therapy[3,15–20].

The photophysical properties of porphyrin compounds have been investigated extensively, both experimentally and theoretically[21–38]. The absorption spectrum of porphyrins features two distinct bands, namely the very bright and rather narrow B band ("Soret band") at about 400 nm and the Q band in the region of 600 - 500 nm which is of moderate intensity[38]. These transitions are commonly rationalized within the Gouterman four-orbital model[39,40]. In D_{2h} nomenclature, combinations of single excitations from two occupied π-orbitals of a_u and b_{1u} symmetry to two virtual π^*-orbitals of b_{2g} and b_{3g} symmetry generate four electronic states, two of B_{3u} symmetry polarized along the x-axis (Q_x and B_x) and two of B_{2u} symmetry polarized along the y-axis (Q_y and B_y). However, the exclusive construction of the B and Q states within the restricted four-orbital basis is in general an inadequate approximation to the low-lying excited states obtained from quantum chemical calculations[34,35,41,42].

The present study is concerned with the photochemical pathways of free-base porphyrins, i.e., metal-free porphyrins. We aim to elucidate the ultrafast photochemistry that is observed experimentally,[21–24] and investigate in the course of the study whether or not the Gouterman model is able to account for these observations. In a study of free-base tetraphenylporphyrin (H_2TPP) by Zewail and collaborators[21], it was shown that excitation to the B band (Soret band) is followed by internal conversion between the B band and the Q band within less than 100 fs. Likewise, time-resolved studies of porphine (H_2P) by Akimoto et al.[22] and Mar-

[a] Institute of Physical and Theoretical Chemistry, Goethe University Frankfurt, Max-von-Laue-Str. 7, 60438 Frankfurt, Germany. E-mail: burghardt@chemie.uni-frankfurt.de
[b] Aix Marseille Univ, CNRS, ICR, 13013 Marseille, France. E-mail: miquel.huixrotllant@univ-amu.fr

celli et al.[23] have reported $B \rightarrow Q$ internal conversion on a time scale ≤ 50 fs (below instrument resolution) followed by $Q_y \rightarrow Q_x$ decay within $\sim$90-150 fs. In a more recent time-resolved fluorescence study of H_2TPP by Joo and collaborators[24], a time scale of $\sim$70 fs for the B state decay was determined and persistent coherent wavepacket motion was observed, indicative of pronounced vibronic coupling effects. From the state-specific nature of the vibrational motions, a competition between a direct $B \rightarrow Q_x$ pathway and a stepwise $B \rightarrow Q_y \rightarrow Q_x$ pathway was inferred. A residual part of the population was found to remain in the Q_y state.

Deexcitation to the electronic ground state is a slow process, mediated by intersystem crossing[26,29,33,43]. Following internal conversion to the Q band, fluorescence is thus observed to some extent,[26,33] while intersystem crossing to the lowest triplet state dominates, on a time scale of $\sim$100 ns[33] (giving rise to weak, long-lived phosphorescence[44]). Excited-state single and double proton transfer is found to play an important role in inducing comparatively rapid intersystem crossing[33]. These proton transfer processes, involving concerted or stepwise tautomerization, are also observed in the ground state[45–49] and induce branching pathways due to low barriers to hydrogen migration within the inner porphyrin ring.

In the present investigation, we focus on the ultrafast (sub-picosecond) photochemistry of free-base porphyrins within the low-lying singlet states. While the abovementioned experimental works[21–24] provide clear evidence for ultrafast $B \rightarrow Q$ internal conversion, the underlying mechanism has not been characterized to date. Given that the B/Q gap is of the order of 1 eV at the Franck-Condon (FC) geometry, conventional energy gap laws[50] cannot be applied.

Against this background, the present computational study aims to clarify the mechanism of $B \rightarrow Q$ internal conversion, focusing upon the simplest prototypical free-base porphyrin, i.e., the porphine (H_2P) compound. To this end, we carried out excited-state electronic structure studies at the level of Time-Dependent Density Functional Theory (TDDFT) as well as complete-active space and second-order perturbation theory (CASSCF/CASPT2) methods, complemented by direct-dynamics surface-hopping simulations to estimate the internal conversion time scales.

2 Computational details

Standard Density Functional Theory (DFT) methodology was employed for the optimization of ground state structures and minima were verified by Hessian analysis. Excited-state minimum energy structures were obtained at the TDDFT level of theory. Single point excited-state analysis was performed at the *ab initio* CASPT2 and XMCQDPT2[51] levels as implemented in MOLCAS 8.0[52] and in the Firefly QC package[53] which is partially based on the GAMESS (US) source code[54]. TDDFT calculations based on optimized DFT structures were obtained using Gaussian09 Rev.D01[55]. A benchmark of the effect of the exchange correlation functional has been performed using a variety of functional types[56–67].

Minimum energy conical intersection (MECI) points were located by means of the branching-plane update method[68] as implemented in GAMESS2014[69] relying on the BH&HLYP func-
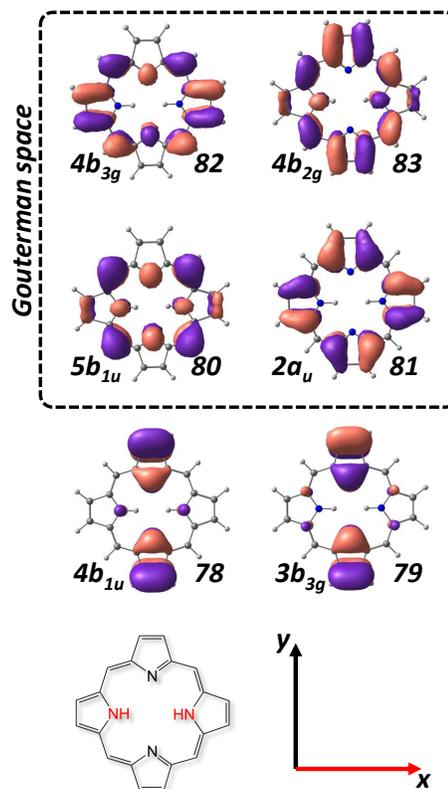

Fig. 1 Porphine frontier orbitals with highlighted Gouterman space (top), energetic order obtained at BH&HLYP/6-31G* level of theory, symmetry assignment according to D_{2h} nomenclature and reference coordinate frame for the free-base porphyrin model compound (bottom).

tional and the Pople 6-31G* basis set which has proven effective in related studies[70–72]. For the MECI searches, the Tamm-Dancoff approximation[73] of TDDFT has been applied. While TDDFT fails in the description of conical intersections with the electronic ground state,[74] the potential energy surface (PES) topology for excited states including conical intersections is described in a correct fashion.[74–76] For the present system, we carried out benchmark studies using CASPT2 and XMCQDPT2 as mentioned above, to validate our TDDFT calculations.

On-the-fly surface-hopping simulations have been conducted via the Newton-X program version 2.0[77,78]. To this end, initial conditions were generated from the DFT-based optimized ground state minimum structures by sampling a Wigner distribution as implemented in Newton-X. A total of 167 trajectories was included the trajectory surface-hopping dynamics simulation. The ratio of trajectories starting from the B_x and B_y states were chosen to match the ratio of oscillator strengths of these states at the ground state minimum structure. TDDFT single-point calculations were carried out at every time step (with $\Delta t = 0.5$ fs, using the standard 5th-order Butcher integrator[77]) of the simulation at the TD-BH&HLYP/6-31G* level, in line with the methodology employed for the static calculations as mentioned before.

Table 1 Excited state spectrum of porphine at the Franck-Condon geometry obtained at different levels of theory for the 6-31G* Pople basis set (a) and the ANO-RCC-VDZ basis set (b), relative energies in eV of the first five excited states, deviations from the Gouterman B and Q state sequence are indicated by the respective irreducible representations

method	S_1	S_2	S_3	S_4	S_5
CAM-B3LYP[a]	2.22	2.44	3.60	3.73	3.95 B_{1g}
M062X[a]	2.30	2.55	3.63	3.73	3.98 B_{1g}
ωB97XD[a]	2.16	2.40	3.60	3.73	3.96 B_{1g}
M06HF[a]	2.04	2.46	3.76	3.82	4.43 B_{1g}
M06[a]	2.26	2.40	3.40	3.57	3.57 B_{1g}
BH&HLYP[a]	2.33	2.51	3.71	3.83	4.09 B_{1g}
B3LYP[a]	2.31	2.47	3.39 B_{1g}	3.48 B_{1g}	3.55
PBE0[a]	2.35	2.51	3.46 B_{1g}	3.60 B_{1g}	3.62
BP86[a]	2.21	2.34	3.02 B_{1g}	3.05	3.06
BLYP[a]	2.20	2.33	3.00 B_{1g}	3.04	3.05
M06L[a]	2.28	2.40	3.22 B_{1g}	3.22	3.27
CAS(4,4)PT2[b]	2.51	3.04	4.27	4.33	–
CAS(8,6)PT2[b]	2.17	2.81	3.83	3.90	3.97 B_{1g}
XMCQDPT2[a]// CAS(10,10)	1.77	2.37	3.08	3.08	3.31 B_{1g}
Exp. [38,82]	1.98–2.02	2.38–2.42	3.13–3.33	3.13–3.33	3.65
	Q_x	Q_y	B_x	B_y	N
CAS(4,4) [34]	3.48	3.71	5.08	5.12	–
SC-NEVPT2 [34]	2.05	2.53	3.25	3.33	–
CAS(14,13) [34]	3.12	3.80	4.72	5.22	5.74
SC-NEVPT2 [34]	2.05	2.56	3.49	3.62	4.10

3 Results and discussion

3.1 Augmented Gouterman model

Throughout the following discussion, the symmetry classification will relate to the porphine molecule of D_{2h} point group located in the xy-plane and the pyrrolic hydrogens oriented along the x-axis as indicated in Fig. 1 in accordance with common nomenclature for this system. The Gouterman frontier orbitals can then be classified in the following representations: $5b_{1u}$ (HOMO-1), $2a_u$ (HOMO), $4b_{3g}$ (LUMO) and $4b_{2g}$ (LUMO+1) respectively. These give rise to the well-known (Q_x, Q_y) and (B_x, B_y) states, see Table 2.

As also shown in Fig. 1, other orbitals will turn out to play an important role, notably the $3b_{3g}$ (HOMO-2) and $4b_{1u}$ (HOMO-3) occupied orbitals. Transitions between these orbitals and the Gouterman type LUMOs $4b_{3g}$ and $4b_{2g}$ are found to appear next to the B band and can therefore significantly influence the photochemistry of the system. These transitions either correspond to spectroscopically observable states assigned to the N band[41,79] (noting that the N, L, and M band are the UV bands lying above the B band[2]) or else related dark states of zero oscillator strength. In line with the convention of Ref. 79, we will refer to the bright N-type states as (N_x, N_y) and to the dark states as (N_{xy}, N_s).

Various DFT functionals and basis sets were tested against benchmark calculations using the CASSCF/CASPT2 and XMC-QDPT2 methods. Since the free-base porphyrin scaffold is rather rigid, all methods yield closely related results for equilibrium geometries, and energies are found to be in good agreement. The influence of the basis set quality also remains limited.

Table 1 presents single-point calculations for the first five singlet states, obtained with various DFT functionals as compared with our CASPT2 and XMCQDPT2 results along with literature benchmarks. The active spaces employed in the multiconfigurational calculations refer to the Gouterman space (4,4) as well the

Table 2 Classification and composition of the first eight excited states of the free-base porphyrin at the Franck-Condon geometry obtained at the TD-BH&HLYP/6-31G* level of theory, cf. Fig. 1 for orbital classification

state	assignment	relative energy (eV)	orbital transitions	oscillator strength
S_1	$1^1B_{3u}(Q_x)$	2.33	$80\ 5b_{1u} \rightarrow 83\ 4b_{2g}$ (0.50)	0.0043
			$81\ 2a_u \rightarrow 82\ 4b_{3g}$ (0.50)	
S_2	$1^1B_{2u}(Q_y)$	2.51	$80\ 5b_{1u} \rightarrow 82\ 4b_{3g}$ (-0.49)	0.0038
			$81\ 2a_u \rightarrow 83\ 4b_{2g}$ (0.51)	
S_3	$2^1B_{3u}(B_x)$	3.71	$78\ 4b_{1u} \rightarrow 83\ 4b_{2g}$ (-0.27)	0.9043
			$80\ 5b_{1u} \rightarrow 83\ 4b_{2g}$ (-0.45)	
			$81\ 2a_u \rightarrow 82\ 4b_{3g}$ (0.48)	
S_4	$2^1B_{2u}(B_y)$	3.83	$80\ 5b_{1u} \rightarrow 82\ 4b_{3g}$ (0.52)	1.2345
			$81\ 2a_u \rightarrow 83\ 4b_{2g}$ (0.49)	
S_5	$1^1B_{1g}(N_{xy})$	4.09	$79\ 3b_{3g} \rightarrow 83\ 4b_{2g}$ (0.68)	0.0000
S_6	$3^1B_{3u}(N_x)$	4.45	$78\ 4b_{1u} \rightarrow 83\ 4b_{2g}$ (0.63)	0.5740
			$80\ 5b_{1u} \rightarrow 83\ 4b_{2g}$ (-0.23)	
			$81\ 2a_u \rightarrow 82\ 4b_{3g}$ (0.19)	
S_7	$2^1A_g(N_s)$	4.53	$79\ 3b_{3g} \rightarrow 82\ 4b_{3g}$ (0.69)	0.0000
S_8	$3^1B_{2u}(N_y)$	4.68	$78\ 4b_{1u} \rightarrow 82\ 4b_{2g}$ (0.68)	0.1166

extended Gouterman space (8,6) shown in Fig. 1; further, the XMCQDPT2 calculations necessitate a larger active space (here, (10,10)) to properly describe higher CI roots (see Table S1 of the Supporting Information).

In most cases, the electronic state assignment corresponds to the sequence $S_1(Q_x)$, $S_2(Q_y)$, $S_3(B_x)$, $S_4(B_y)$, $S_5(N_{xy})$ at the Franck-Condon geometry. However, interchanges among the S_3, S_4 and S_5 states occur for certain functionals, as indicated in the Table. Notably, the dark state 1^1B_{1g} (N_{xy}) ($3b_{3g} \rightarrow 4b_{2g}$), can be found to be intercalated into the B band. This effect is slightly more pronounced for standard hybrid functionals than for long-range corrected methods. Additionally, local functionals show even more significant relative stability of the above dark state $1^1B_{1g}(N_{xy})$ which is now sandwiched between the Q and B states at the Franck-Condon geometry accompanied by an energetic decrease of the $3^1B_{3u}(N_x)$ state. However, the evaluation of the state character by excited state properties, especially the oscillator strength, is not unambiguous for the local functionals. Combined with the fact that the energetic gap between the Q and B bands is also underestimated substantially in these cases, this class of functionals will be discarded from the present discussion.

Regarding previously reported high level *ab initio* benchmark calculations[34,80] caution is advised as far as quantitative experimental agreement goes, as the results displayed in Table 1 reveal. Increasing the active space does not necessarily yield satisfactory results whereas perturbation correction usually leads to a drastic improvement to capture significant amounts of electronic correlation. However, state composition and character may be very sensitive to variations of the reference CI wave function. Typically, only spectroscopically bright states have been discussed in this context[35,42,80,81].

For the detailed PES studies described in the following, we select the TD-BH&HLYP/6-31G* exchange correlation functional, which yields results in satisfactory agreement with our CASPT2 reference calculations as far as the energetics and state characters are concerned. This choice is a compromise in that TD-

Table 2 illustrates the classification of the first eight excited states at the Franck-Condon geometry, based on the BH&HLYP functional. Besides the (Q_x, Q_y) and (B_x, B_y) transitions, different types of additional transitions arise. These include the spectroscopically dark transitions 1^1B_{1g} $(3b_{3g} \rightarrow 4b_{2g})$ and 1^1A_g $(3b_{3g} \rightarrow 4b_{2g})$ which we identify as N_{xy} and N_s, respectively, following the assignment by Cai *et al.*[79], as well as the transitions $3^1B_{3u}(N_x)$ and $3^1B_{2u}(N_y)$ that can be assigned to the spectroscopically observable N band.

In view of a discussion of the photochemical pathways initiated by excitation into the B band, we augment the Gouterman model such as to account for these additional N type states. As shown in Table 2, the augmented set of six orbitals depicted in Fig. 1 is mandatory to account for the full set of transitions involved in the internal conversion.

By inspecting electronic transitions such as $^1B_{1g}(N_{xy})$ $(3b_{3g} \rightarrow 4b_{2g})$, we note that these additional states differ qualitatively from the Gouterman Q and B states in two ways: (i) the transitions are basically single transitions in contrast to the equally weighted superpositions of two Gouterman type transitions for the B and Q states and (ii) the donor orbitals $3b_{3g}$ and $4b_{1u}$ are more localized (interpretable as a combination of non-bonding lone-pair nitrogen orbitals and localized π-orbitals on distinct pyrrolic units of the porphine) as opposed to the largely delocalized Gouterman type frontier orbitals (i.e., $5b_{1u}$, $2a_u$, $4b_{3g}$ and $4b_{2g}$). It is therefore to be expected that geometric distortion of the porphine scaffold will affect the two types of states in quite a different fashion, thus giving rise to possible PES crossings mediated by these additional dark states. In contrast, we expect the B and Q states to respond in a similar fashion to structural variations, resulting in largely parallel PESs, such that marked distortions will be necessary to induce B/Q crossings.

It is further important to point out that while the transition from the $4b_{1u}$ (HOMO-3) orbital to the Gouterman LUMOs contributes to the B_x transition to a non-negligible extent, there is no such trend for the transition from the $3b_{3g}$ (HOMO-2) orbital. At the Franck-Condon geometry, the $^1B_{1g}(N_{xy})$ $(3b_{3g} \rightarrow 4b_{2g})$ state is a pure dark state, whose oscillator strength is strictly zero. By contrast, the $^1B_{3u}(N_x)$ $(4b_{1u} \rightarrow 4b_{2g})$ state is electronically mixed with the B band. However, this will be seen to change at geometries far from the Franck-Condon point – notably when approaching the conical intersection geometries to be discussed below – where the orbitals $3b_{3g}$ and $4b_{1u}$ evolve into independent π-orbitals on distinct pyrrolic units.

3.2 Photochemical pathways

In order to explore photochemical pathways including the dark N type states, critical points of the excited-state PESs were optimized to shed some light onto the possible conical intersection funnels that facilitate the ultrafast relaxation. We anticipate that

A
3.76 (3.66) ___ S_3 / S_2 (N_{xy}/Q_y)

B
4.22 (4.16) ___ S_2 / S_1 (N_{xy}/Q_x)

C
5.13 (5.11) ___ S_3 / S_2 (B_x/Q_y)
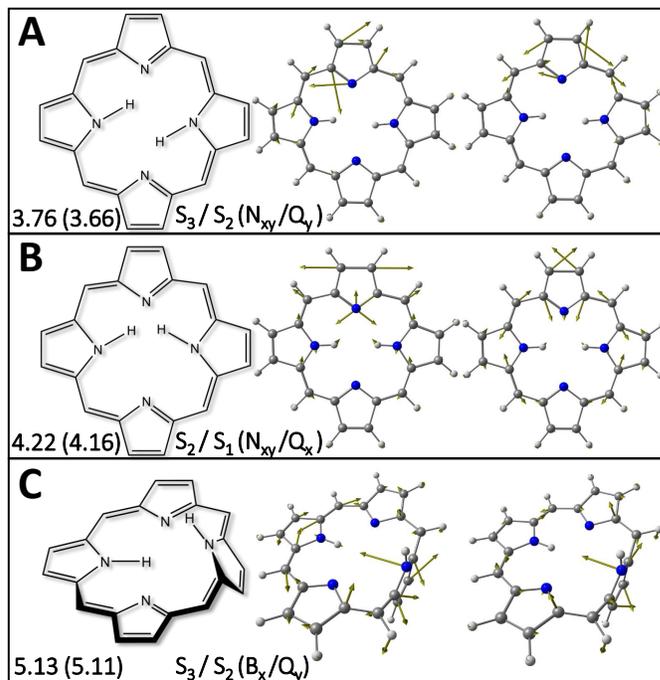
Fig. 2 Optimized minimum energy conical intersection geometries obtained at the TDA-BH&HLYP/6-31G* level of theory: **A**: N_{xy}/Q_y conical intersection; **B**: N_{xy}/Q_x conical intersection; **C**: high energy B_x/Q_y conical intersection. The panels show sketched Lewis structures (left), and the branching plane vectors, i.e., the gradient difference vector X_1 (middle) and the derivative coupling vector X_2 (right). Energies are indicated in eV relative to the Franck-Condon optimized ground state energy; energies in brackets indicate TD-BH&HLYP/6-31G* energies calculated at the TDA-BH&HLYP/6-31G* optimized MECI geometries. (Note the slight red shift of the TDDFT energies.)

various PES crossings could occur relating to both direct $B \rightarrow Q$ and sequential $B \rightarrow N \rightarrow Q$ pathways. Fig. 2 depicts several relevant MECI structures with their respective energies relative to the Franck-Condon ground state. Structural deformations are sketched to emphasize the relevant effective reaction coordinates.

As one of the main findings of this study, it turns out that the energetically accessible conical intersection which is of key importance for $B \rightarrow Q$ internal conversion is *not* a direct B/Q intersection, but rather an intersection of N_{xy}/Q_y character between the S_3 and S_2 states (panel **A** of Fig. 2). Preceding the passage through this intersection, the S_3 state character undergoes an adiabatic transition from B_x to N_{xy}, in a crossing region involving the S_3, S_4, and S_5 states close to the Franck-Condon geometry. The energy predicted for the N_{xy}/Q_y conical intersection lies at approximately 3.76 eV and involves only a slight pyrrolic proton shift in the xy-plane of the porphine. A somewhat more pronounced displacement in the same direction induces an additional Q_y/Q_x crossing at lower energies (2.96 eV). The latter crossing can also be optimized as a MECI. This type of geometry change would therefore favor a sequential downhill $N_{xy} \rightarrow Q_y \rightarrow Q_x$ pathway.

An additional conical intersection structure at approximately 4.2 eV (panel **B** of Fig. 2) opens up another photochemical branch that induces direct $N_{xy} \rightarrow Q_x$ population transfer. This pathway is less favorable energetically than the $N_{xy} \rightarrow Q_y$ transfer, but should be in reach if sufficient excess energy is available.

Finally, a conical intersection permitting direct $B \rightarrow Q$ transfer – without participation of the intermediate dark N_{xy} state – is obtained at very high energy (5.13 eV) and is characterized by a large geometric distortion (out-of-plane bending of a pyrrolic unit), see panel **C**. This conical intersection is unlikely to be reached upon Franck-Condon excitation of the B band.

To illustrate the energetics, Fig. 3 shows PES cuts along a linear interpolation coordinate connecting the Franck-Condon geometry with the N_{xy}/Q_y type MECI between the S_3 and S_2 states. Results obtained at the TDDFT level are compared with XMCQDPT2 reference results, showing good agreement, even though energy gaps may differ sigificantly (notably, the Q_y/Q_x gap is significantly smaller in the TDDFT calculations). As can be inferred from the figure, the S_3 state changes adiabatically from B_x to the dark state N_{xy}. (Note that this change of electronic character is not related to the intrinsic mixing of the B_x state with the N_x state, see Table 2.) The N_{xy} state in turn intersects with the Q states, as explained above.

From the PES cuts and the optimized MECI structures, the following mechanistic route for the internal conversion process can be inferred: After initial photoexcitation to the B band the porphine molecule undergoes minor structural rearrangements (in the porphyrin plane) that induce a smooth transition from the Gouterman B_x state to the dark N_{xy} state. In the adiabatic picture, the PES crossing that induces this change of character near the Franck-Condon geometry involves the S_3, S_4 and S_5 states. The path towards the conical intersection(s) of the N_{xy} state with the Q states is found to be essentially barrierless, and entirely circumvents the high-energy B/Q intersection at 5.13 eV.

The present picture is in line with the spectroscopic study of H$_2$P by Akimoto et al. [22] and Marcelli et al. [23] as well as the study
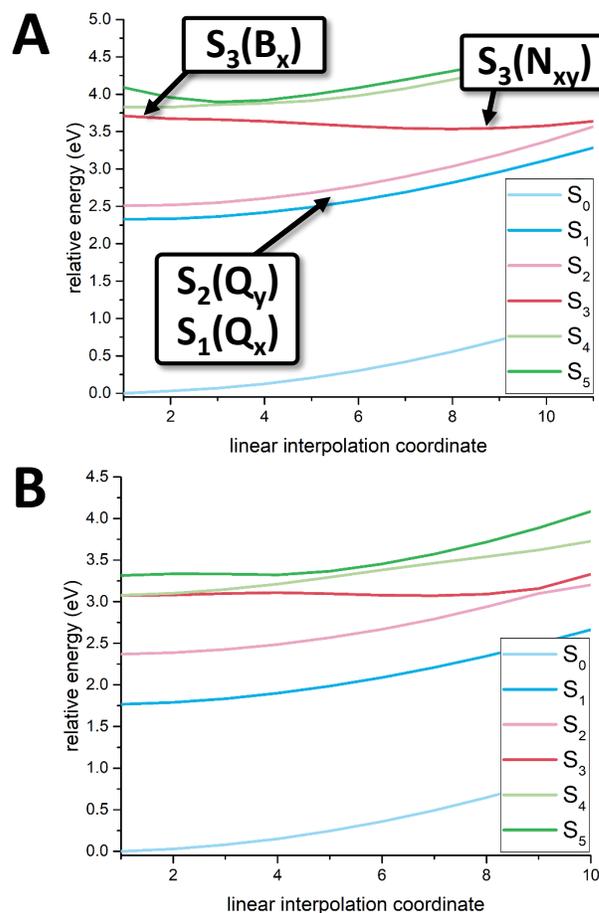
Fig. 3 Potential surface cut along the linear interpolation coordinate (in arbitrary units) connecting the Franck-Condon minimum geometry (left) and the N_{xy}/Q_y conical intersection (right) obtained at TD-BH&HLYP/6-31G* (panel **A**) and at XMCQDPT2/CASSCF(10,10)/6-31G* (panel **B**). Note that the electronic character of the adiabatic S_3 state changes smoothly from B- to N-type along the coordinate as indicated in the upper panel.
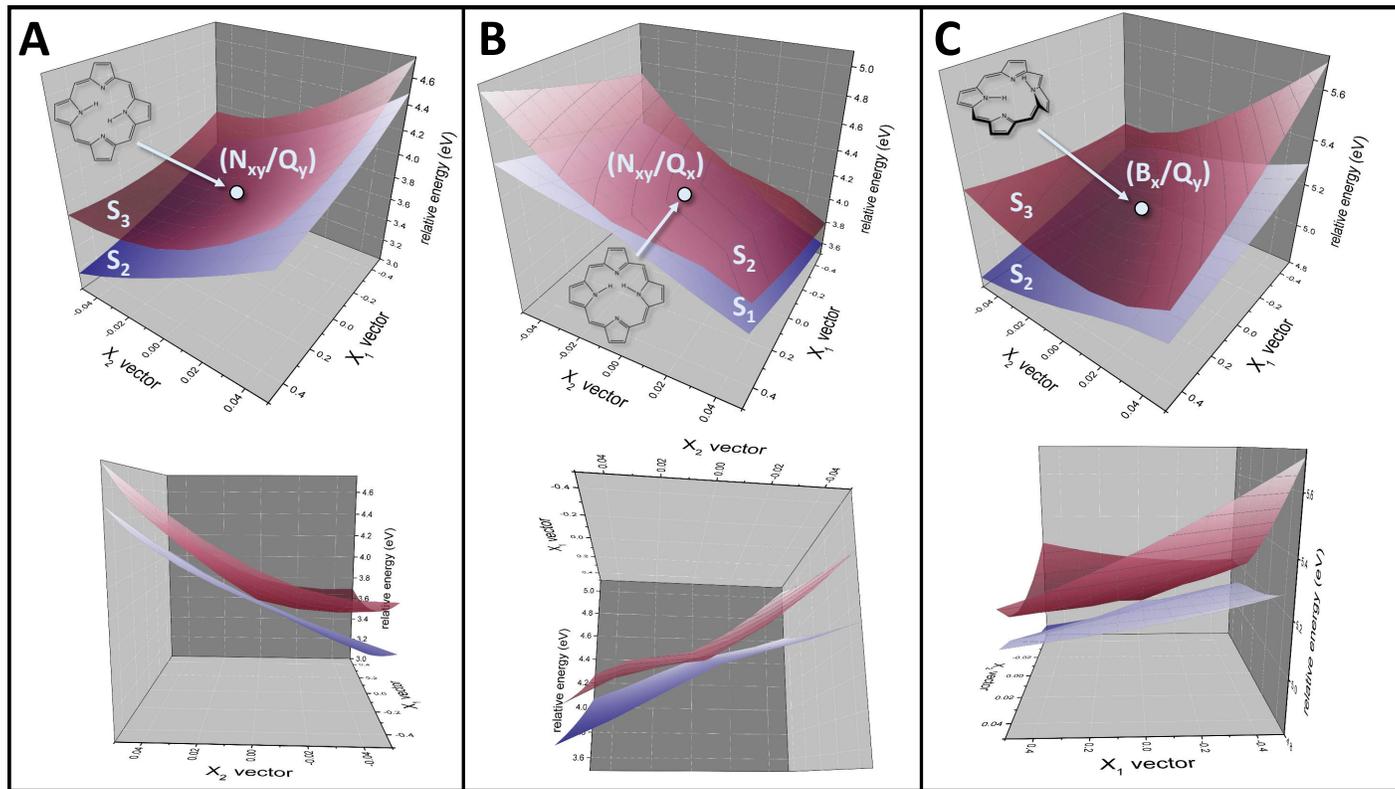
Fig. 4 Two dimensional surface scans of crossing states in the geometric vicinity of their conical intersections spanned by the branching plane vectors X_1 and $X_2$ (top and sideview), obtained at TDA-BH&HLYP/6-31G* level of theory. **A**: N_{xy}/Q_y conical intersection, **B**: N_{xy}/Q_x conical intersection, **C**: B_x/Q_y conical intersection; note that the latter is less sloped.

of H_2TPP by Kim and Joo[24] where an ultrafast B/Q internal conversion process was observed, and an interplay of direct $B \rightarrow Q_x$ and stepwise $B \rightarrow Q_y \rightarrow Q_x$ pathways was inferred from time-resolved experiments. Importantly, our analysis shows that these pathways entirely rely on the mixing between the B band and the dark N states, giving a new interpretation to the experimental findings.

The topologies of the relevant conical intersections discussed above are depicted in Fig. 4. All intersections are found to be of sloped character. Note that the relative energy at the conical intersection is within close range of the B band excitation of 3.7 to 3.8 eV at a similar level of theory. Solvation effects were taken into account via the Polarizable Continuum Model (PCM) model for aromatic solvents (benzene) but are found to be negligible. Further computational considerations are summarized in the Supporting Information.

3.3 Nonadiabatic on-the-fly surface-hopping calculations

In order to verify the above photochemical scenario, mixed quantum-classical trajectory surface-hopping simulations have been conducted. To this end, the Newton-X protocol[77,78] for the surface-hopping procedure was employed. First, initial conditions were prepared for an ensemble of 167 trajectories in the B_x and the B_y states, respectively, *via* sampling of a Wigner distribution in the ground state. Subsequently transition energies were obtained at the TD-DFT level and the generated structures were evaluated

according to standard energetic threshold ranges ($\pm$ 0.5 eV) to be passed on to the surface-hopping dynamics. The simulation time was set to 300 fs with a stepsize of 0.5 fs. At each time step, 11 states (including the ground state) were computed. The ratio of trajectories starting from the B_x and B_y states, respectively, was chosen to match the relative weight of their oscillator strengths in the B band at the Franck-Condon geometry of the optimized molecule.

As can inferred from Fig. 5, the initial kinetics involves a complex interplay of several relaxation channels as discussed above. Panel **A** of Fig. 5 shows the time-evolving populations of the S_n, $n = 1, \ldots, 4$ states which can be identified at the FC geometry as $S_1(Q_x)$, $S_2(Q_y)$, $S_3(B_x)$, and $S_4(B_y)$. The $S_3(B_x)$ state is seen to initially gain population from the $S_4(B_y)$ state within approximately 50 fs, while the trajectories are close to the Franck-Condon region. Transfer to the $S_2(Q_y)$ and $S_1(Q_x)$ states sets in within the first 20 fs, and the combined S_1/S_2 state population starts to exceed the S_3/S_4 state population within less than 100 fs. From a fit of the average S_3/S_4 population (see Fig. S10 of the Supporting Information), we infer a B state decay time of $\tau \simeq 100$ fs, in good agreement with experiments for H_2P[22,23] and H_2TPP[21,24]. As expected, the observed trajectory dynamics involves the in-plane displacements leading to the conical intersection structures of Fig. 2 and Fig. 4 (see the trajectory movie provided in the Supporting Information).

Panel **B** of Fig. 5 illustrates the key role of the S_5 state, which can be identified as the dark $S_5(N_{xy})$ state at the FC geometry.
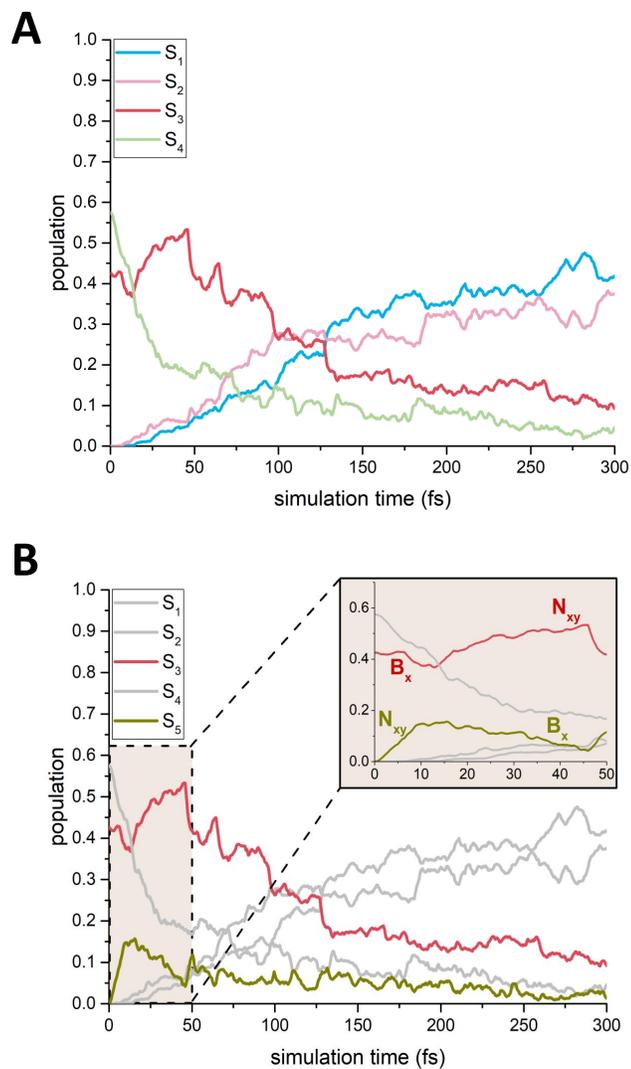
Fig. 5 Adiabatic state populations throughout the dynamics simulation, carried out at the TD-BH&HLYP/6-31G* level, with 167 trajectories and weighted initial conditions according to the B_y/B_x ratio of oscillator strengths. Panel **A**: State populations for S_n, $n = 1, \ldots, 4$, with the state characters $S_1(Q_x)$, $S_2(Q_y)$, $S_3(B_x)$, and $S_4(B_y)$ at the FC geometry, panel **B**: State populations for S_n, $n = 1, \ldots, 5$, where the S_3 and S_5 states are highlighted, noting that $S_5(N_{xy})$ is the N-band dark state that exchanges its electronic character with the S_3 state near the FC geometry, within less than 20 fs (see inset).

Within less than 20 fs, the $S_5(N_{xy})$ and $S_3(B_x)$ states strongly interact near the FC geometry and exchange their electronic character (see inset of Fig. 5**B**), as predicted from the electronic structure analysis of Fig. 3**A**. Following this step, the S_3 state – now of $S_3(N_{xy})$ character – continues to evolve towards the N_{xy}/Q_y conical intersection as discussed above.

While the $S_2(Q_y)$ and $S_1(Q_x)$ state populations both start to build up within the first tens of femtoseconds, one should note that the $S_2(Q_y)$ build-up is predominant until about 120 fs. This is in line with our above observations, where the N_{xy}/Q_y intersection was found to be energetically favorable, while the N_{xy}/Q_x intersection also contributes. These observations match the experimental results for H_2TPP[24], where both direct and sequential pathways towards Q_x were observed. The final S_2 (Q_y) population, however, is still substantial in comparison to experimental results. This effect might stem from the fact that density functional-based methodology tends to underestimate the Q state energy gap, leading to similar time-dependent populations and sustained quantum beats between the Q_x and Q_y states as observed in Fig. 5. (Note that by comparison, our *ab initio* CASPT2 reference calculations comprising an active space as proposed in Fig. 1 drastically overestimate the Q gap, see Fig. 3 and Fig. S8 of the Supporting Information.)

A Jablonski-type mechanistic diagram of the overall process is displayed in Fig. 6, to summarize the main aspects of this study. After initial photoexcitation to the B band, followed by quantitative transfer to the lower B_x state, the population is directed towards the Q band by means of ultrafast internal conversion. Importantly, this process is induced by the mixing with dark N states. Several conical intersections are involved that require little geometric distortion and are therefore readily accessible within reasonable energetic ranges. Sequential $B \to N \to Q_y \to Q_x$ and $B \to N \to Q_x$ pathways interfere on a time scale of about 100 fs. The intramolecular cascade does not involve direct B/Q transfer as a result of the extremely unfavorable energetics of the relevant conical intersection.

4 Conclusions

The present study highlights that the ultrafast internal conversion between the B states and the Q states of porphine necessitates an analysis of the electronic structure beyond the conventional Gouterman picture. While a direct internal conversion pathway exists between the B and Q states, this route is energetically highly unfavorable and involves an out-of-plane motion of one of the pyrrolic rings. In contrast, an almost barrierless internal conversion process is mediated by dark states belonging to the N manifold. This process involves minimal displacements of in-plane vibrations, and is found to induce an ultrafast dynamics with participation of both sequential $B \to N \to Q_y \to Q_x$ and direct $B \to N \to Q_x$ transitions. Various conical intersections are found to mediate the ultrafast decay.

The spectroscopically dark N type states which act as intermediate states in the $B \to Q$ internal conversion have been previously described at the Franck-Condon geometry[41,79], but their role in the photochemistry of porphine has not been investigated. Indeed, to the best of our knowledge, the present study offers the
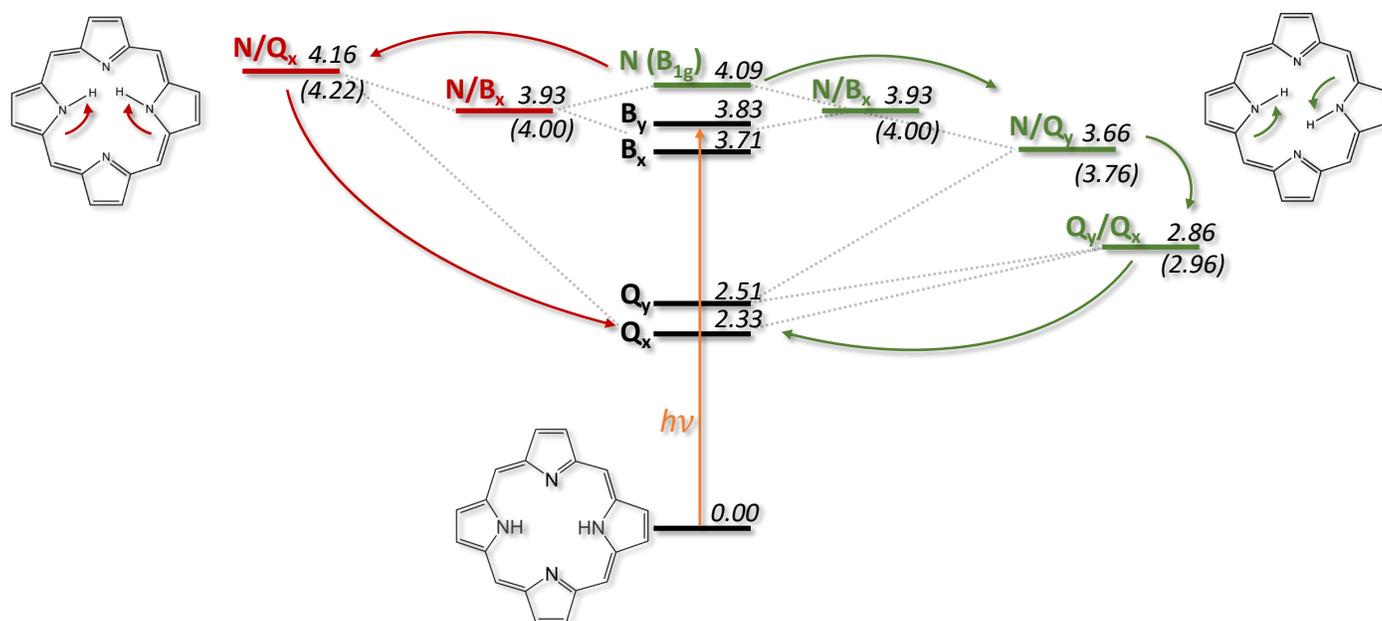
Fig. 6 Main intramolecular relaxation channels of porphine proposed in this study. Relative energies obtained at the TD-BH&HLYP/6-31G* level of theory are indicated in eV; energies in brackets show MECI energies obtained at the TDA level, see Fig. 2. A photochemical cascade is observed that mediates population transfer from the B band via the dark N_{xy} state to the Q band involving several conical intersections. Grey dotted lines indicate the electronic entanglement of the respective states along the effective relaxation coordinate. The green pathway emphasizes the energetically favorable sequence while the red branch depicts the unfavorable, high-energetic route towards direct population of the Q_x state.

first consistent picture of ultrafast $B \to Q$ internal conversion.

The time scale of B state decay of $\sim$100 fs observed in our on-the-fly surface-hopping calculations is in good agreement with the time-resolved studies of H_2P by Akimoto et al.[22] and Marcelli et al.[23] as well as related studies of the H_2TPP system by Joo and collaborators[24], who report a decay of the B state within $\leq$ 100 fs. Likewise, our time-dependent simulations agree with the latter study regarding the observation of interleaved sequential $B \to N \to Q_y \to Q_x$ and direct $B \to N \to Q_x$ pathways, as mentioned above. Preferential passage via the sequential pathway can be explained by the favorable energetics of the conical intersection between the intermediate N type states and the Q_y states.

However, our analysis is not conclusive with regard to state-specific vibrational signatures as observed in the time-resolved fluorescence study of H_2TPP by Joo and collaborators[24]. In this study, persistent and state-specific oscillations with frequencies around $\sim$30 cm^{-1} and $\sim$190 cm^{-1} were recorded within an observation window of 3 ps and attributed to out-of-plane porphyrin modes. While typical in-plane modes that mediate the passage through the conical intersections discussed above also include this frequency range, our current time-dependent simulations (within a window of 300 fs) do not permit to analyse the participation of specific modes. Furthermore, the mixed quantum-classical surface-hopping technique that has been employed may not be suitable to describe coherent wavepacket dynamics on these extended time scales accurately.

Follow-up studies are planned to parametrize a vibronic coupling model Hamiltonian in view of a full quantum dynamical treatment, guided by the results of the present surface-hopping study. Furthermore, we will expand the present study to various substituted species, to investigate the validity of the present mechanism for a broad class of porphyrins, and examine possible cases where the intermediate dark states are photochemically inactive. Notably, Marcelli et al.[23] report that $B \to Q$ internal conversion increases to a time scale of 10-25 ps in diprotonated porphine derivatives, suggesting that the $B \to N \to Q$ pathway is inactive in these species.

To summarize, the present study provides a consistent mechanistic picture of the complex multi-state pathways of $B \to Q$ internal conversion in porphine. The present results are likely relevant for the whole class of free-base porphyrins and open a new avenue for the understanding of photochemical processes in porphyrin-based nanostructured assemblies.

Conflicts of interest

There are no conflicts to declare.

Acknowledgments

Notes and references

1 Battersby, A. R.; Fookes, C. J. R.; Matcham, G. W. J.; McDonald, E. *Nature* **1980**, *285*, 17–21, 10.1038/285017a0.

2 Dolphin, D. *Structure and synthesis*; The Porphyrins; Acad. Press, 1978.

3 Garrot, D.; Langlois, B.; Roquelet, C.; Michel, T.; Roussignol, P.; Delalande, C.; Deleporte, E.; Lauret, J.-S.; Voisin, C. *J. Phys. Chem. C* **2011**, *115*, 23283–23292.

4 Ding, Y.; Zhu, W.; Xie, Y. *Chem. Rev.* **2017**, *117*, 2203.

5 Dasler, D.; Schäfer, R. A.; Minameyer, M. B.; Hitzenberger, J. F.; Hauke, F.; Drewello, T.; Hirsch, A. *J. Am. Chem. Soc.* **2017**, *139*, 11760–11765.

6 Wolf, M.; Herrmann, A.; Hirsch, A.; Guldi, D. M. *J. Am. Chem. Soc.* **2017**, *139*, 11779–11788.

7 Giardina, B.; Messana, I.; Scatena, R.; Castagnola, M. *Crit. Rev. Biochem. Mol. Biol.* **1995**, *30*, 165–196.

8 Shanmugathasan, S.; Edwards, C.; Boyle, R. W. *Tetrahedron* **2000**, *56*, 1025–1046.

9 Shelby, M. L.; Lestrange, P. J.; Jackson, N. E.; Haldrup, K.; Mara, M. W.; Stickrath, A. B.; Zhu, D.; Lemke, H. T.; Chollet, M.; Hoffman, B. M.; Li, X.; Chen, L. X. *Journal of the American Chemical Society* **2016**, *138*, 8752–8764.

10 Govind, C.; Karunakaran, V. *J. Phys. Chem. B* **2017**, *121*, 3111–3120.

11 Awasabisah, D.; Xu, N.; Gautam, K. P. S.; Powell, D. R.; Shaw, M. J.; Richter-Addo, G. B. *Eur. J. Inorg. Chem.* **2016**, *2016*, 509–518.

12 Rury, A. S.; Wiley, T. E.; Sension, R. J. *Acc. Chem. Res.* **2015**, *48*, 860–867.

13 Consani, C.; Auböck, G.; Bräm, O.; van Mourik, F.; Chergui, M. *J. Chem. Phys.* **2014**, *140*, 025103.

14 Khairutdinov, R.; Serpone, N. *J. Phys. Chem. B* **1999**, *103*, 761.

15 Castano, A. P.; Demidova, T. N.; Hamblin, M. R. *Photodiagn. Photodyn. Ther.* **2004**, *1*, 279–293.

16 Nyman, E. S.; Hynninen, P. H. *J. Photochem. Photobiol., B* **2004**, *73*, 1–28.

17 Orellana, W. *Appl. Phys. Lett.* **2014**, *105*, 023110.

18 Orellana, W.; Correa, J. D. *J. Mater. Sci.* **2015**, *50*, 898–905.

19 Orellana, W. *Chem. Phys. Lett.* **2015**, *634*, 47–52.

20 Jurow, M.; Schuckman, A. E.; Batteas, J. D.; Drain, C. M. *Coord. Chem. Rev.* **2010**, *254*, 2297–2310.

21 Baskin, J. S.; Yu, H.-Z.; Zewail, A. H. *J. Phys. Chem. A* **2002**, *106*, 9837–9844.

22 Akimoto, S.; Yamazaki, T.; Yamazaki, I.; Osuka, A. *Chem. Phys. Lett.* **1999**, *309*, 177-182.

23 Marcelli, A.; Foggi, P.; Moroni, L.; Gellini, C.; Salvi, P. R. *J. Phys. Chem. A* **2008**, *112*, 1864–1872.

24 Kim, S. Y.; Joo, T. *J. Phys. Chem. Lett.* **2015**, *6*, 2993–2998.

25 Abraham, B.; Nieto-Pescador, J.; Gundlach, L. *J. Phys. Chem. Lett.* **2016**, *7*, 3151–3156.

26 Valiev, R. R.; Cherepanov, V. N.; Artyukhov, V. Y.; Sundholm, D. *Phys. Chem. Chem. Phys.* **2012**, *14*, 11508–11517.

27 Liang, Y.; Bradler, M.; Klinger, M.; Schalk, O.; Balaban, M. C.; Balaban, T. S.; Riedle, E.; Unterreiner, A.-N. *ChemPlusChem* **2013**, *78*, 1244–1251.

28 Bialkowski, B.; Stepanenko, Y.; Nejbauer, M.; Radzewicz, C.; Waluk, J. *J. Photochem. Photobiol., A* **2012**, *234*, 100–106.

29 Yeon, K. Y.; Jeong, D.; Kim, S. K. *Chem. Commun.* **2010**, *46*, 5572–5574.

30 Yu, H.-Z.; Baskin, J. S.; Zewail, A. H. *J. Phys. Chem. A* **2002**, *106*, 9845–9854.

31 Kay, C. W. M. *J. Am. Chem. Soc.* **2003**, *125*, 13861–13867.

32 Palummo, M.; Hogan, C.; Sottile, F.; Bagala, P.; Rubio, A. *J. Chem. Phys.* **2009**, *131*, 084102.

33 Perun, S.; Tatchen, J.; Marian, C. M. *ChemPhysChem* **2008**, *9*, 282–292.

34 Angeli, C.; Pastore, M.; Cimiraglia, R. *Theor. Chem. Acc.* **2007**, *117*, 743–754.

35 Merchán, M.; Ortí, E.; Roos, B. O. *Chem. Phys. Lett.* **1994**, *226*, 27–36.

36 Nagashima, U.; Takada, T.; Ohno, K. *J. Chem. Phys.* **1986**, *85*, 4524–4529.

37 Gouterman, M. *J. Chem. Phys.* **1959**, *30*, 1139–1161.

38 Edwards, L.; Dolphin, D. H.; Gouterman, M.; Adler, A. D. *J. Mol. Spectrosc.* **1971**, *38*, 16–32.

39 Gouterman, M. *J. Mol. Spectrosc.* **1961**, *6*, 138–163.

40 Gouterman, M.; Wagnière, G. H.; Snyder, L. C. *J. Mol. Spectrosc.* **1963**, *11*, 108–127.

41 Sundholm, D. *Phys. Chem. Chem. Phys.* **2000**, *2*, 2275–2281.

42 Serrano-Andrés, L.; Merchán, M.; Rubio, M.; Roos, B. O. *Chem. Phys. Lett.* **1998**, *295*, 195–203.

43 Mandal, A. K.; Taniguchi, M.; Diers, J. R.; Niedzwiedzki, D. M.; Kirmaier, C.; Lindsey, J. S.; Bocian, D. F.; Holten, D. *J. Phys. Chem. A* **2016**, *120*, 9719–9731.

44 Minaev, B.; Agren, H. *Chem. Phys.* **2005**, *315*, 215.

45 Waluk, J. *Acc. Chem. Res.* **2006**, *39*, 945–952.

46 Waluk, J. *Chem. Rev.* **2017**, *117*, 2447–2480.

47 Koch, M.; Pagan, M.; Persson, M.; Gawinkowski, S.; Waluk, J.; Kumagai, T. *J. Am. Chem. Soc.* **2017**, *139*, 12681–12687.

48 Sobolewski, A. L.; Gil, M.; Dobkowski, J.; Waluk, J. *J. Phys. Chem. A* **2009**, *113*, 7714–7716.

49 Albareda, G.; Bofill, J. M.; Tavernelli, I.; Huarte-Larranaga, F.; Illas, F.; Rubio, A. *J. Phys. Chem. Lett.* **2015**, *6*, 1529–1535.

50 Englman, R.; Jortner, J. *Mol. Phys.* **1970**, *18*, 145.

51 Granovsky, A. A. *J. Chem. Phys.* **2011**, *134*, 214113.

52 Aquilante, F.; Autschbach, J.; Carlson, R. K.; Chibotaru, L. F.; Delcey, M. G.; Vico, L. D.; Galván, I. F.; Ferré, N.; Frutos, L. M.; Gagliardi, L.; Garavelli, M.; Giussani, A.; Hoyer, C. E.; Manni, G. L.; Lischka, H.; D. Ma, P. A. M.; Müller, T.; Nenov, A.; M. Olivucci, T. B. P.; Peng, D.; Plasser, F.; Pritchard, B.; Reiher, M.; Rivalta, I.; Schapiro, I.; Segarra-Martí, J.; Stenrup, M.; Truhlar, D. G.; Ungur, L.; Valentini, A.; Vancoillie, S.; Veryazov, V.; Vysotskiy, V. P.; Weingart, O.; Zapata, F.; Lindh, R. MOLCAS 8: New Capabilities for Multiconfigurational Quantum Chemical Calculations across the Periodic Table. Journal of Computational Chemistry, 37, 506-541, 2016.

53 Granovsky, A. A. Firefly version 8. www http://classic.chem.msu.su/gran/firefly/index.html.

54 Schmidt, M. W.; Baldridge, K. K.; Boatz, J. A.; Elbert, S. T.; Gordon, M. S.; Jensen, J. H.; Koseki, S.; Matsunaga, N.; Nguyen, K. A.; Su, S.; Windus, T. L.; Dupuis, M.; Montgomery, J. A. *J. Comput. Chem.* **1993**, *14*, 1347–1363.

55 Frisch, M. J.; Trucks, G. W.; Schlegel, H. B.; Scuseria, G. E.; Robb, M. A.; Cheeseman, J. R.; Scalmani, G.; Barone, V.; Mennucci, B.; Petersson, G. A.; Nakatsuji, H.; Caricato, M.; Li, X.; Hratchian, H. P.; Izmaylov, A. F.; Bloino, J.; Zheng, G.; Sonnenberg, J. L.; Hada, M.; Ehara, M.; Toyota, K.; Fukuda, R.; Hasegawa, J.; Ishida, M.; Nakajima, T.; Honda, Y.; Kitao, O.; Nakai, H.; Vreven, T.; Montgomery, J. A., Jr.; Peralta, J. E.; Ogliaro, F.; Bearpark, M.; Heyd, J. J.; Brothers, E.; Kudin, K. N.; Staroverov, V. N.; Kobayashi, R.; Normand, J.; Raghavachari, K.; Rendell, A.; Burant, J. C.; Iyengar, S. S.; Tomasi, J.; Cossi, M.; Rega, N.; Millam, J. M.; Klene, M.; Knox, J. E.; Cross, J. B.; Bakken, V.; Adamo, C.; Jaramillo, J.; Gomperts, R.; Stratmann, R. E.; Yazyev, O.; Austin, A. J.; Cammi, R.; Pomelli, C.; Ochterski, J. W.; Martin, R. L.; Morokuma, K.; Zakrzewski, V. G.; Voth, G. A.; Salvador, P.; Dannenberg, J. J.; Dapprich, S.; Daniels, A. D.; Farkas, Ö.; Foresman, J. B.; Ortiz, J. V.; Cioslowski, J.; Fox, D. J. Gaussian 09 Revision D.01. Gaussian Inc. Wallingford CT.

56 Yanai, T.; Tew, D. P.; Handy, N. C. *Chem. Phys. Lett.* **2004**, *393*, 51–57.

57 Zhao, Y.; Truhlar, D. G. *Theor. Chem. Acc.* **2008**, *120*, 215–241.

58 Chai, J.-D.; Head-Gordon, M. *Phys. Chem. Chem. Phys.* **2008**, *10*, 6615–6620.

59 Zhao, Y.; Truhlar, D. G. *J. Phys. Chem. A* **2006**, *110*, 5121–5129.

60 Zhao, Y.; Truhlar, D. G. *J. Phys. Chem. A* **2006**, *110*, 13126–13130.

61 Becke, A. D. *J. Chem. Phys.* **1993**, *98*, 1372–1377.

62 Lee, C.; Yang, W.; Parr, R. G. *Phys. Rev. B* **1988**, *37*, 785–789, PRB.

63 Becke, A. D. *J. Chem. Phys.* **1993**, *98*, 5648–5652.

64 Adamo, C.; Barone, V. *J. Chem. Phys.* **1999**, *110*, 6158–6170.

65 Becke, A. D. *Phys. Rev. A* **1988**, *38*, 3098–3100, PRA.

66 Perdew, J. P. *Phys. Rev. B* **1986**, *33*, 8822–8824, PRB.

67 Zhao, Y.; Truhlar, D. G. *J. Chem. Phys.* **2006**, *125*, 194101.

68 Maeda, S.; Ohno, K.; Morokuma, K. *J. Chem. Theory Comput.* **2010**, *6*, 1538–1545.

69 M.W.Schmidt,; K.K.Baldridge,; J.A.Boatz,; S.T.Elbert,; M.S.Gordon,; J.H.Jensen,; S.Koseki,; N.Matsunaga,; K.A.Nguyen,; S.Su,; T.L.Windus,; M.Dupuis,; J.A.Montgomery, GAMESS VERSION 5 (DEC 2014 (R1), General Atomic and Molecular Electronic Structure System. J. Comput. Chem., 14, 1347-1363, 1993.

70 Almlof, J.; Fischer, T. H.; Gassman, P. G.; Ghosh, A.; Haeser, M. *J. Phys. Chem.* **1993**, *97*, 10964–10970.

71 Hehre, W. J.; Ditchfield, R.; Pople, J. A. *J. Chem. Phys.* **1972**, *56*, 2257–2261.

72 Nikiforov, A.; Gamez, J. A.; Thiel, W.; Huix-Rotllant, M.; Filatov, M. *J. Chem. Phys.* **2014**, *141*, 124122.

73 Hirata, S.; Head-Gordon, M. *Chem. Phys. Lett.* **1999**, *314*, 291–299.

74 Levine, B. G.; Ko, C.; Quenneville, J.; Martínez, T. J. *Mol. Phys.* **2006**, *104*, 1039–1051.

75 Tapavicza, E.; Tavernelli, I.; Rothlisberger, U.; Filippi, C.; Casida, M. E. *J. Chem. Phys.* **2008**, *129*, 124108.

76 Wohlgemuth, M.; Bonačić-Koutecký, V.; Mitrić, R. *J. Chem. Phys.* **2011**, *135*, 054105.

77 Barbatti, M.; Granucci, G.; Persico, M.; Ruckenbauer, M.; Vazdar, M.; Eckert-Maksić, M.; Lischka, H. *J. Photochem. Photobiol., A* **2007**, *190*, 228–240.

78 Barbatti, M.; Ruckenbauer, M.; Plasser, F.; Pittner, J.; Granucci, G.; Persico, M.; Lischka, H. *Wiley Interdiscip. Rev.: Comput. Mol. Sci.* **2014**, *4*, 26–33.

79 Cai, Z.-L.; Crossley, M. J.; Reimers, J. R.; Kobayashi, R.; Amos, R. D. *J. Phys. Chem. B* **2006**, *110*, 15624–15632.

80 Kerridge, A. *Phys. Chem. Chem. Phys.* **2013**, *15*, 2197–2209.

81 Baerends, E. J.; Ricciardi, G.; Rosa, A.; van Gisbergen, S. J. A. *Coord. Chem. Rev.* **2002**, *230*, 5–27.

82 Kim, B. F.; Bohandy, J. *J. Mol. Spectrosc.* **1978**, *73*, 332–343.